metals

MDPI

Article

Modifying Microstructure and Mechanical Properties of Mo-Nb Single Crystals via Thermal Annealing

Li Huang, Wen Zhang *, Zhongwu Hu, Tao Yin, Linjiang Guo and Hanyu Zheng

Northwest Institute for Nonferrous Metal Research, Xi'an 710016, China; huangli46272@163.com (L.H.); huzhongwu123@aliyun.com (Z.H.); yintao0808@163.com (T.Y.); xbyglj@163.com (L.G.); zhenghanyu1991@163.com (H.Z.)
* Correspondence: gwenzh@163.com

Abstract: Molybdenum-Niobium (Mo-Nb) single crystals possess excellent mechanical properties, such as high strength and low creep rate at high temperatures, which leads to Mo-Nb single crystals' potential application in the irradiated and aerospace environment. Mechanical properties at high temperatures are closely related to structural defects, including the density of dislocation and low-angle grain boundaries in a single-crystal Mo alloy. It is well known that the density of defects is mainly contributed to by processing and annealing. To clarify the microstructural evolution of Mo-Nb single-crystal alloys, thermal annealing tests with temperatures varying from 1100 °C to 1700 °C were conducted. Two Nb contents (3 at.% and 6 at.%) were chosen to investigate the effect of Nb content on the thermal stability (≤1700 °C) of single-crystal Mo-Nb alloys. Samples with high Nb content (6 at.%) soften after annealing, while ductility at room temperature obviously enhances In the low Nb content (3 at.%) sample, however, hardening and softening occur after low (1100 °C) and high temperature annealing, respectively. The evolution of mechanical properties could be mainly attributed to the change of density in the low-angle grain boundary. Furthermore, the changing Nb element and dislocation density during annealing are still important to the strength and ductility of Mo-Nb single crystals.

Keywords: Mo-Nb alloys; single crystal; microstructure; mechanical properties; thermal annealing

check for updates

Citation: Huang, L.; Zhang, W.; Hu, Z.; Yin, T.; Guo, L.; Zheng, H. Modifying Microstructure and Mechanical Properties of Mo-Nb Single Crystals via Thermal Annealing. *Metals* **2023**, *13*, 1261. https://doi.org/10.3390/met13071261

Academic Editor: Andrey Belyakov

Received: 17 May 2023
Revised: 8 June 2023
Accepted: 21 June 2023
Published: 13 July 2023

Copyright: © 2023 by the authors. Licensee MDPI, Basel, Switzerland. This article is an open access article distributed under the terms and conditions of the Creative Commons Attribution (CC BY) license (https://creativecommons.org/licenses/by/4.0/).

1. Introduction

Molybdenum possesses both high physical and mechanical properties, such as good structural stability, thermal conductivity, and high strength at high temperatures [1]. Its highly stable body-centered cubic (BCC) structure makes multi-strengthening methods possible in molybdenum alloys. The effective improvement of strength and creep resistance at high temperatures could be obtained via solution strengthening (Zr, Ti [2], Nb, W [3], Si [4], and B [5]), dispersion strengthening (MoTiC [6], HfC [7], La_2O_3 [8,9], WC [10], ZrC [11] et al.), and the combination of these two strengthening methods [12]. High mechanical properties at high temperatures have been achieved in some Mo alloys, such as ZrC-strengthened Mo alloys [11]. Thermal stability is a key factor to determine the service life because Mo alloys are often used in high temperature environments. Thermal stability can also be successfully approached and, importantly, guided by theoretical works, especially by ab initio molecular dynamics (AIMD) [13,14]. Researchers employ AIMD to successfully deal with thermal stability and mechanical properties in 2D materials.

Although a large amount of research has been conducted, the structural stability and reliability of Mo alloys at high temperatures for a pretty long time are still doubtful. To obtain a high requirement of stability, single crystals for refractory alloys are becoming the most potential choices in the future. Among lots of refractory alloys, MoNb single crystals possess excellent structural stability and mechanical properties at high temperatures [15]. The high preference for Mo alloy single crystals is attributed to the relatively low stored energy that is caused by the low density of dislocations and small-angle grain boundaries [16].

As a typical domestic refractory system, the microstructures and mechanical properties of MoNb single crystals have been widely investigated [17–19]. Slip behavior and dislocation arrangements are carefully justified under compression at room temperature [17]. For compression at high temperatures, structural stability in MoNb single crystals rises as the Nb content increases [18]. What is more, researchers have compressively compared the difference in mechanical responses between single crystals and poly-crystals [3].

Although they contain excellent properties at high temperatures, the mechanical properties of Mo single crystals, especially the ductility at room temperature, still need to be improved. Among many methods, one of the most effective ways to enhance mechanical properties is adding Rhenium to Mo alloys [19]. Considering the high cost of Rhenium, thermal annealing is another usual way to enhance the mechanical properties [20–22]. Lowry et al. showed that the theoretical strength of Mo alloys with defect-free crystals is obtained via proper heat treatment [20]. In Yang et al.'s results, dislocations are from excess vacancy during the annealing treatment and play important roles for precipitates in Mo-12Si-8.5B alloys [21]. However, in Hiraoka's results, the embrittlement after annealing at 1500 °C is mainly due to the proceeding of second-phase precipitation followed by a substantial hardening in Mo-40% Ru alloy [22].

Here, firstly, the structural evolution and mechanical properties of Mo alloys' single crystals via adding Nb are investigated. Secondly, the effect of thermal annealing on the mechanical properties of MoNb single crystals is considered and discussed. Mo and MoNb alloys single crystals are prepared via the electron beam zone-melting method. The annealing temperature is in the range of 1100 °C to 1700 °C. The annealing time is maintained for 2 h to ensure uniform heating. The tensile tests at room temperature and structural evolutions before and after annealing are carefully investigated in this research, in order to evaluate the influence of thermal annealing on the mechanical properties of MoNb alloys' single crystals.

2. Materials and Methods

Mo and Mo-Nb single crystals were prepared via mixing high pure Mo and Nb powders, followed by the pressing, sintering, and electron beam zone-melting methods. The Nb content of Mo-Nb single crystals are 3 at.% and 6 at.%, hereafter abbreviated as Mo3Nb and Mo6Nb, respectively. Subsequently, Mo3Nb and Mo6Nb single crystals were vacuum annealed at 1100 °C, 1300 °C, 1500 °C, and 1700 °C for 2 h with a vacuum degree higher than 1×10^{-4} Pa. The microstructural features of all samples were detected by X-ray diffraction (XRD) and metallurgical microscope. The samples used for metallurgical microscope observation were prepared via mechanically grinding, polishing, and chemically corroding to make the low-angle grain boundary easy to detect.

To investigate the effect of thermal annealing on mechanical properties, rod tension samples with a diameter of 3 mm and a length of 30 mm at the work region were made by machine work. To make the test reliable, spiral burrs were processed at both edges of the tensile sample. Tensile tests were performed at room temperature with a strain rate of 1.67×10^{-3} s^{-1}. Tests were conducted until a fracture occurred with a constant strain rate. Three tests were done for each sample to ensure the results. After tensile tests, fracture sections were observed via scanning electron microscope (SEM). Furthermore, microstructural details, such as dislocation features after deformation, were characterized by transmission electron microscopy (TEM) operating at 200 KV. The foils for TEM were polished mechanically under 50 μm thickness and thinned by a twinjet electro-polisher in an electrolyte of 75 mL CH_3OH + 25 mL H_2SO_4 at 223 K and at voltage 25 V. The elemental distributions were detected via an energy dispersive spectrometer (EDS) in TEM.

3. Results

XRD patterns for casted Mo, Mo3Nb, and Mo6Nb are shown in Figure 1a. The 2θ ranges from 20° to 120°. Only 222 peaks are detected at ~117° (an extinction of light occurs at 111 orientation). Such features not only justify the growing direction is 111,

but also prove the single crystal body-centered cubic (BCC) structure for all samples. Although the lattice misfit is enhanced as the Nb content increases, the structural stability is maintained after adding 6 at.% content. Figure 1b,c, respectively, show the microstructural evolution of Mo3Nb and Mo6Nb after thermal annealing at 1100 °C, 1300 °C, 1500 °C, and 1700 °C for 2 h. Still, only 222 peaks are detected at ~117° in all annealed samples. The same features of casted and annealed Mo3Nb and Mo6Nb suggest no recrystallization occurs, which means a high thermal stability (≤1700 °C) of Mo and MoNb single crystals.

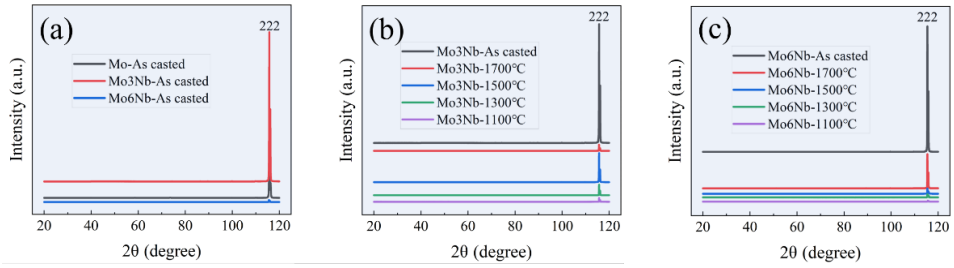


Figure 1. XRD patterns of Mo, Mo3Nb, and Mo6Nb before and after thermal annealing. As-casted Mo, Mo3Nb, and Mo6Nb are shown in (**a**), annealed Mo3Nb and Mo6Nb are shown in (**b**,**c**), respectively.

To observe the evolution of the low-angle grain boundary after annealing, metallographic photos of Mo3Nb single crystals were taken and are shown in Figure 2. The reticular wave lines on the surface of MoNb single crystals are known as the low-angle grain boundary. Figure 2a shows the distribution of the low-angle grain boundary for as-casted Mo3Nb single crystals. Low density in the center part and a relatively higher density at the edge were observed, which is consistent with the thermal diffusion direction. The density of the low-angle grain boundary in Mo3Nb rises after annealing at 1100 °C, as shown in Figure 2b. Then, the density of the low-angle grain boundary drops after annealing at high temperatures, as shown in Figure 2c,d. As shown in Figure 2c, the low-angle grain boundary in the center part dramatically decreases. For the samples after 1700 °C annealing, nearly all of the wave lines are absent, as shown in Figure 2d.

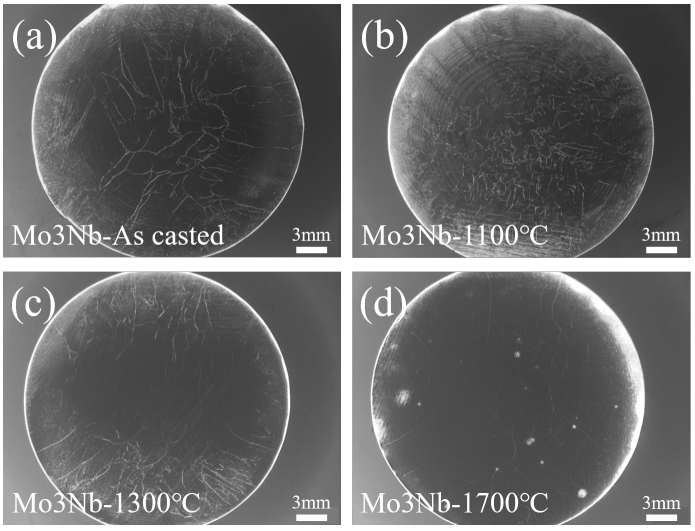


Figure 2. Metallographic images of as-casted and annealed Mo3Nb single crystals. As-casted Mo3Nb is shown in (**a**); 1100 °C annealed Mo3Nb is shown in (**b**); 1300 °C annealed Mo3Nb is shown in (**c**); 1700 °C annealed Mo3Nb is shown in (**d**), respectively.

Figure 3 shows the evolution of the low-angle grain boundary of Mo6Nb single crystals before and after annealing. Comparing with as-casted Mo3Nb, the density of the low-angle grain boundary obviously elevates in as-casted Mo6Nb, as shown in Figures 2a and 3a.

This is consistent with the higher lattice misfit in Mo6Nb than in Mo3Nb single crystals. The low-angle grain boundary density decreases as the annealing temperature increases, as shown in Figure 3a–d. After 1700 °C annealing, no low-angle grain boundary was detected in Mo6Nb, as shown in Figure 3d, which is the same as Mo3Nb.

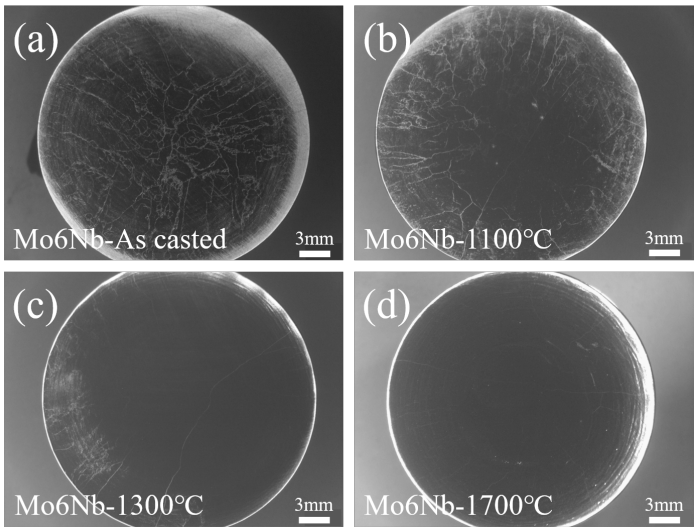


Figure 3. Metallographic images of as-casted and annealed Mo6Nb single crystals. As-casted Mo6Nb is shown in (**a**); 1100 °C annealed Mo6Nb is shown in (**b**); 1300 °C annealed Mo6Nb is shown in (**c**); 1700 °C annealed Mo6Nb is shown in (**d**), respectively.

These results in Figures 2 and 3 mean that both Nb content and annealing temperature influence the microstructure of MoNb single crystals. The main difference between Mo3Nb and Mo6Nb is the structural evolution after 1300 °C annealing, which may relate to the zone-melting process. In annealing tests at high temperatures (1500 °C and 1700 °C), the low-angle grain boundary density drops in both Mo3Nb and Mo6Nb, which may be contributed to by a diffusion-induced defect evolution.

Figure 4 shows the tensile results of Mo and MoNb single crystals. Figure 4a–c are true strain-true stress curves for Mo, Mo3Nb, and Mo6Nb, respectively. Three tests were given for every group to ensure tensile results. Mo single crystals yield at nearly 300 MPa. Then, true stress continues to rise as true strain increases. The maximum stress reaches 550 MPa at true strain ~5%, as shown in Figure 4a. Mo3Nb single crystals yield at ~400 MPa. A small stress drop occurs after yield and the maximum stress reaches 600 MPa, as shown in Figure 4b. The yield point in Mo6Nb single crystals is 450 MPa, which is nearly the same as the maximum stress, as shown in Figure 4c.

Figure 4d shows representative Mo, Mo3Nb, and Mo6Nb curves, in order to compare different deformation features. No obvious difference was observed among the three curves before yield, suggesting a small content of Nb addition has little influence on the elastic contacts of Mo. Yield happens in Mo single crystals first. Then, true stress increases slowly as the strain continues, as shown in Figure 4a. For Mo3Nb single crystals, true stress drops ~20 MPa at 1% strain after yield, followed by a gentle rise during subsequent loading, as shown in Figure 4b. Yield enhances as the Nb content increases. Mo6Nb possesses higher strength (~450 MPa) than Mo3Nb and Mo. Furthermore, the stress in Mo6Nb maintains at a relatively stable level until failure, as shown in Figure 4c,f, which means a stable flow and dislocation movement. Severe work hardening occurs in Mo3Nb at true strain ranges from 1.5% to ~5%, and then, softening occurs and stress drops quickly until failure, as shown in Figure 4e. The true stress maintains a stable value after yield to fracture, which suggests a relatively uniform plastic flow. In summary, the addition of Nb not only enhances the strength of Mo but also improves the stability of mechanical properties.

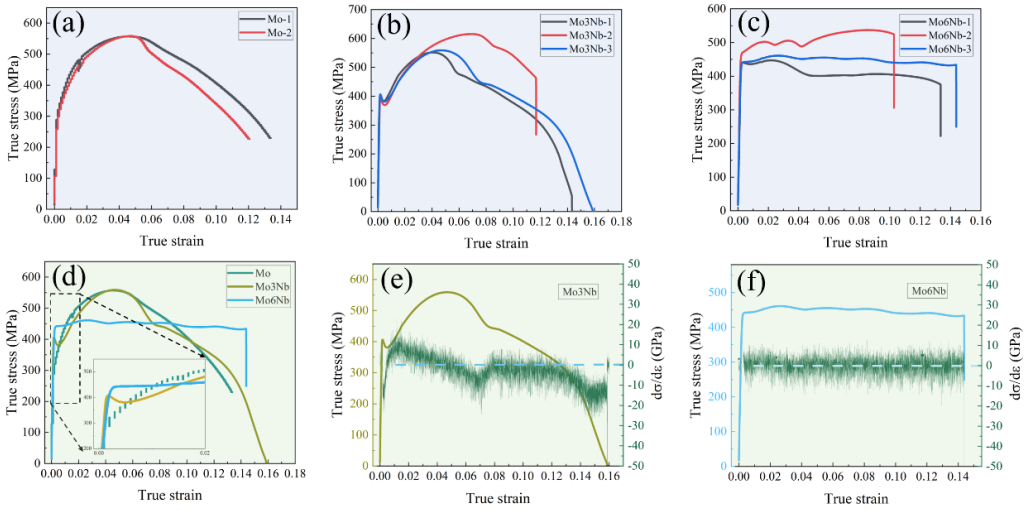


Figure 4. Tensile results of as-casted Mo, Mo3Nb, and Mo6Nb single crystals. (**a**–**c**) are true stress-true strain curves of as-casted Mo, Mo3Nb, and Mo6Nb, respectively; (**d**) is a combination of representative Mo, Mo3Nb, and Mo6Nb curves. Work-hardening rates of Mo3Nb and Mo6Nb are shown in (**e**,**f**), respectively.

Representative true stress-true strain curves of Mo3Nb and Mo6Nb after annealing are shown in Figure 5a,b, respectively. Thermal annealing has little effect on the deformation features, such as elastic to plastic regions and work-hardening behavior. An outstanding behavior in Mo3Nb single crystals is the stress drop after yield, which disappears after annealing at 1700 °C. Such behavior is related to dislocation de-pinned at the yield point. Annealing at 1700 °C makes solute atoms distribute more uniformly than as-casted Mo3Nb single crystals.

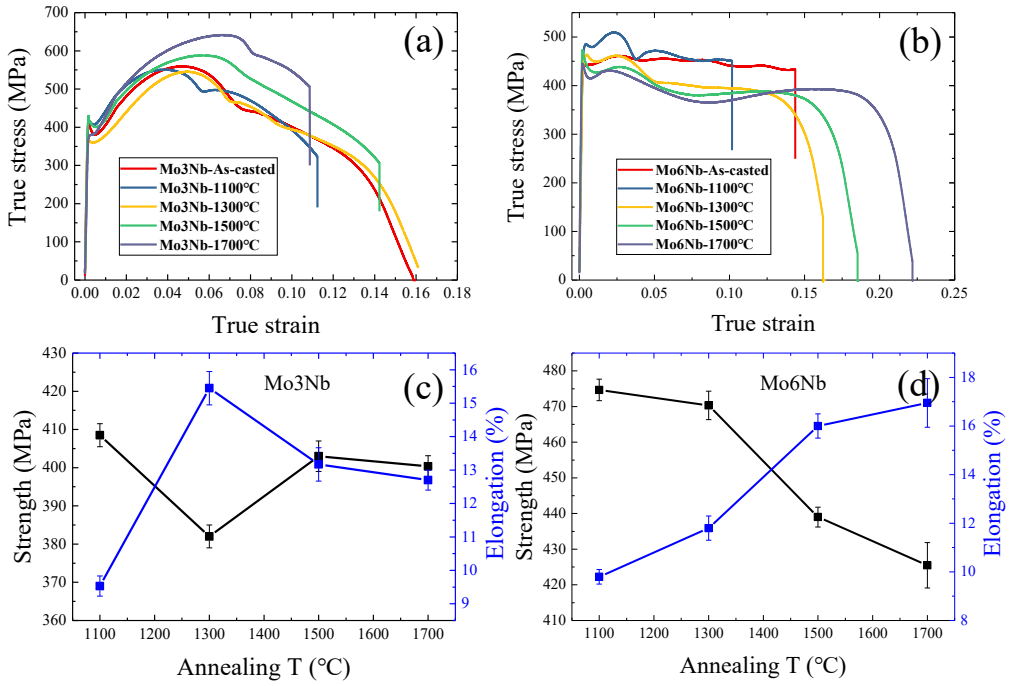


Figure 5. Tensile results of annealed Mo, Mo3Nb, and Mo6Nb single crystals. (**a**,**b**) are true stress-true strain curves of annealed Mo3Nb and Mo6Nb, respectively; (**c**,**d**) are the evolution of strength as annealing temperatures in Mo3Nb and Mo6Nb, respectively.

What is more, strength and elongation change a lot after annealing. Figure 5c,d shows the evolution of strength and elongation in Mo3Nb and Mo6Nb as the annealing

temperature rises, respectively. Comparing with the as-casted sample (yield strength ~410 MPa and elongation 10.9%), the yield strength in Mo3Nb does not change so much after annealing. For example, the yield strength is 405 MPa after 1700 °C annealing. Elongation, however, enhances notably after annealing, especially at 1300 °C annealing. The yield stress in Mo6Nb single crystals decreases continuously as the annealing temperature rises. The strength of Mo6Nb decreases from ~475 MPa at the 1100 °C annealed sample to ~425 MPa at the 1700 °C annealed sample. Meanwhile, the elongation of Mo6Nb increases from ~10% at the 1100 °C annealed sample to ~17% at the 1700 °C annealed sample.

Figure 6 shows microscopes of fracture surfaces after tension. The fracture surface section in Mo3Nb looks like a thin line at the edge. The middle part shows river patterns that suggest inhomogeneous deformation, as shown in the insert (a-I). Such a kind of feature is caused by severe shrinkage in one direction, but relatively small shrinkage in another direction. In Figure 6b, the 1700 °C annealed Mo3Nb behaves the same fracture mode with the as-casted Mo3Nb. Still, some defects, such as holes, were detected near the middle part of the fracture section. The area of the fracture surface is larger in the 1700 °C annealed Mo6Nb than in the as-casted one.

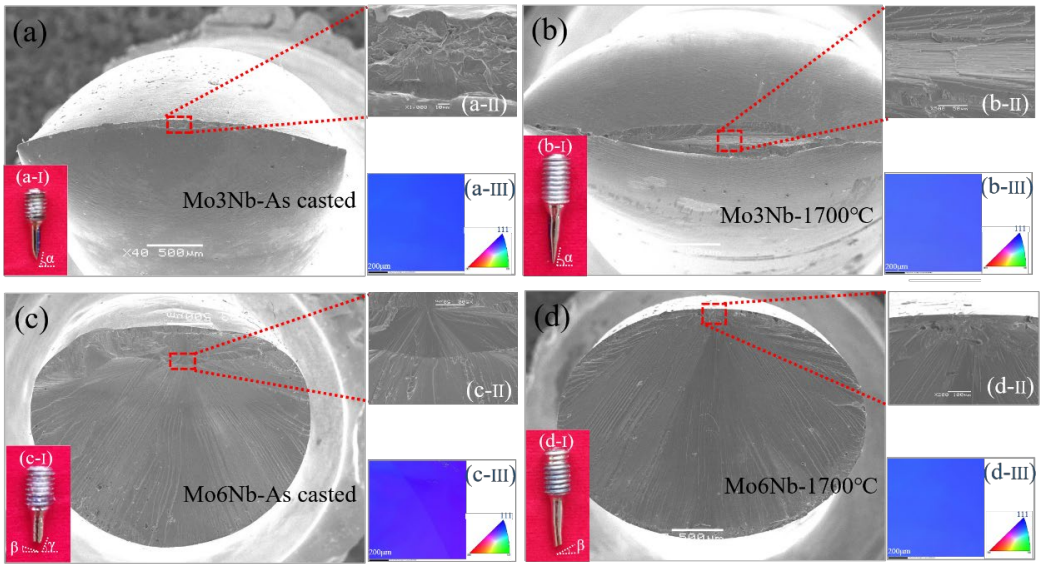


Figure 6. SEM patterns of fracture surfaces after tension at room temperature. (**a**–**d**) are the fractures of as-casted Mo3Nb, 1700 °C annealed Mo3Nb, as-casted Mo6Nb, and 1700 °C annealed Mo6Nb, respectively. The inserts (**a-I**), (**a-II**), and (**a-III**) in (**a**) are the picture of a part of the cracked sample, the magnification of the red square in (**a**), and the EBSD result after the tension, respectively, which is the same corresponding relation between those charts in (**b**–**d**).

Distinguishing from the fracture feature in Mo3Nb, the fracture surface of the as-casted Mo6Nb is like an oval, as shown in Figure 6c. That means the difference between the shrinkage of the two vertical directions in Mo6Nb is much smaller than Mo3Nb. It is noted that those river patterns extend from a small region near the surface with some holes around it, as shown in Figure 6d. In general, as-casted Mo6Nb shows a similar fracture feature in the 1700 °C annealed sample, except that the river patterns initiate in the inner part. The fracture angles are signed as α in the insert of Figure 6a,b, and are signed as β and γ in the insert of Figure 6c,d. The fracture angle still means there is a different deformation mode between Mo3Nb and Mo6Nb single crystals.

The inserts of Figure 6(a-III,b-III,c-III,d-III) are EBSD results of as-casted Mo3Nb, 1700 °C annealed Mo3Nb, as-casted Mo6Nb, and 1700 °C annealed Mo6Nb, respectively. All deformed samples only show the 111 texture, and no recrystallization is observed. Therefore, Mo3Nb and Mo6Nb single crystals possess good mechanical properties and

high structural stability during tension at room temperature. The ductility of Mo3Nb and Mo6Nb are both enhanced to some extent after thermal annealing.

Figure 7 shows TEM figures of deformed samples. All images are observed along the 111 zone axis. Many tangled dislocation lines are observed in the deformed samples. There are some differences in the density of dislocation. Firstly, the density of dislocation in the 1700 °C annealed Mo3Nb is less than in the as-casted Mo3Nb. The width between the two groups of tangled dislocations in the as-casted Mo3Nb (W_1 in Figure 7a) is thinner than in the 1700 °C annealed Mo3Nb (W_2 in Figure 7b). Such a trend means some dislocations have been removed via annealing at 1700 °C. Secondly, the dislocation density in the 1700 °C annealed Mo6Nb is less than in the 1700 °C annealed Mo3Nb, which may lead to a higher strength in Mo6Nb than Mo3Nb. Figure 7d,g shows the magnifications of the dislocation feature in Figure 7a. $\vec{g}$ in Figure 7d,g are $01\bar{1}$ and 110, respectively. Those white dotted lines in Figure 7d represent dislocation lines that are visible in Figure 7d, but invisible in Figure 7g. Thus, those dislocations in Figure 7d should have $\vec{b}$ $\frac{1}{2}1\bar{1}1$. There are still some tangled dislocations that have not been justified. The magnifications of the dislocation feature in Figure 7a are shown in Figure 7e,h. Two long dislocations signed as dotted lines have $\vec{b}$ $\frac{1}{2}1\bar{1}1$. The corresponding dotted lines in Figure 7f,i still have $\vec{b}$ $\frac{1}{2}1\bar{1}1$. Less tangled dislocation is observed in the 1700 °C annealed Mo6Nb than in the 1700 °C annealed Mo3Nb, which is ensured via Figure 7e,f.

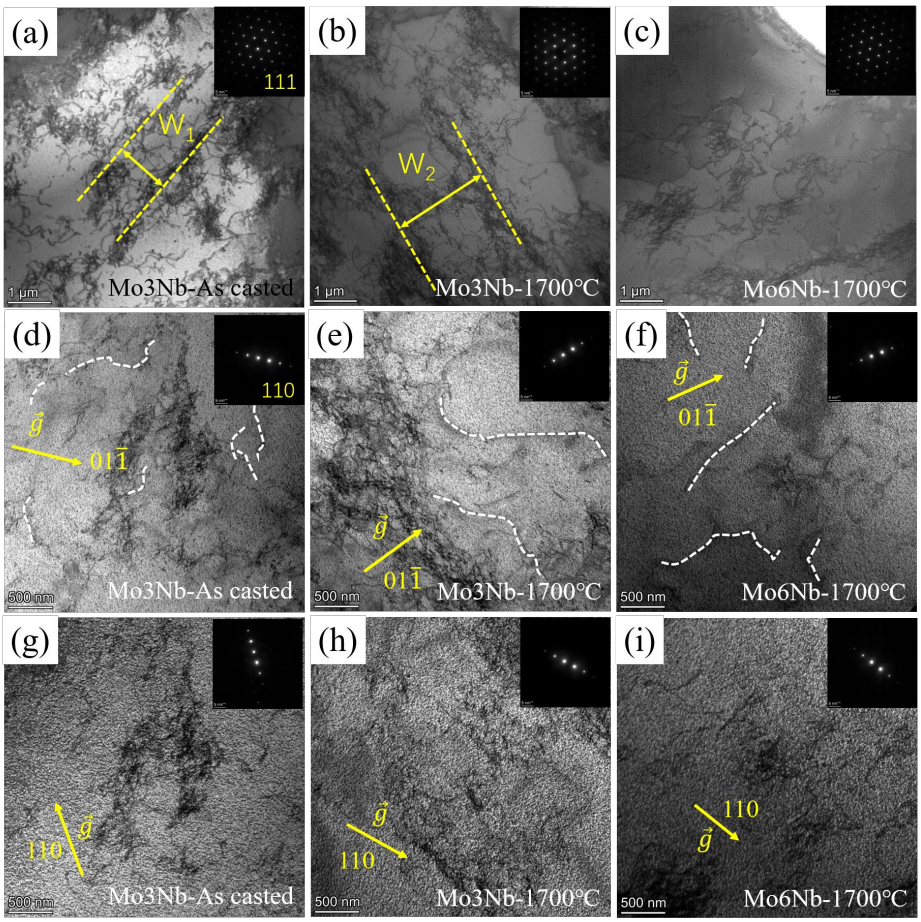


Figure 7. TEM results of as-casted Mo3Nb, 1700 °C annealed Mo3Nb, and 1700 °C annealed Mo6Nb. (**a**–**c**) are images with beam direction 111. The beam directions in (**d**–**f**) are 110 with $\vec{g}01\bar{1}$. The beam directions in (**g**–**i**) are 110 with $\vec{g}$ 110.

Figure 8 shows the line-scanning EDS data along dislocations in the as-casted Mo3Nb, the 1700 °C annealed Mo3Nb, the as-casted Mo6Nb, and the 1700 °C annealed Mo6Nb.

The white lines in the middle of the TEM images show the positions of the dislocations. There is no obvious fluctuation in Mo in all of the samples, as shown in the red figures in Figure 8. The fluctuation in Re, however, is less severe in the as-casted Mo3Nb than in Mo6Nb, as shown in Figure 8a,c. After annealing at 1700 °C, Nb fluctuates smoothly in both Mo3Nb and Mo6Nb, meaning Nb distributes more uniformly after 1700 °C annealing. In detail, the dislocation in the as-casted Mo3Nb has a bit concentration of Nb, which is eliminated after annealing at 1700 °C, as shown in Figure 8a,b. In the as-casted Mo6Nb, the Nb content around the dislocation is a little higher than the matrix. Similar to Mo3Nb, the Nb concentration in dislocation is eliminated to a large extent after annealing. Therefore, thermal annealing makes the microstructure more homogeneous than the as-casted Mo-Nb single crystals.

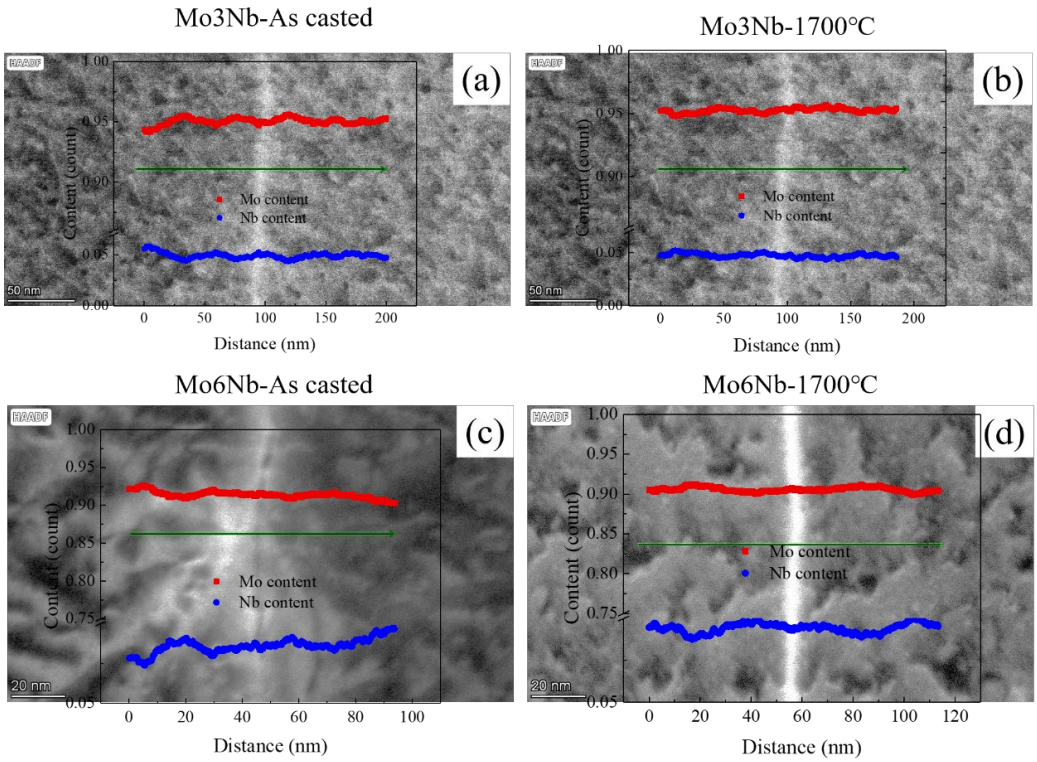


Figure 8. EDS results of as-casted Mo3Nb in (**a**); 1700 °C annealed Mo3Nb in (**b**); as-casted Mo6Nb in (**c**); and 1700 °C annealed Mo6Nb in (**d**), respectively.

4. Discussion

As-casted Mo3Nb and Mo6Nb have different fracture directions along with loading directions, as shown α and α + β in inserts (a-I) and (c-I) in Figure 6. α, β, and γ are ~70°, ~20°, and ~55°, respectively. The loading directions are all 111 in the above-mentioned results, and $\vec{b}$ $\frac{1}{2}1\bar{1}1$ is justified via TEM figures in Figure 7. Furthermore, the dislocations that activated at room temperature in Mo are always screw features [23]. Thus, the slip directions in both Mo3Nb and Mo6Nb single crystals are the same with $\vec{b}$. Those slip systems are likely to be (110)<1$\bar{1}$1>, (011)<1$\bar{1}$1>, (121)<1$\bar{1}$1>, (2$\bar{1}$1)<1$\bar{1}$1>, and (1$\bar{1}$2)<1$\bar{1}$1>. The {123}<111> slip systems are not considered here because those are rarely observed in BCC metals at room temperature [24,25]. Combining the possible systems and fracture features (α, β, and γ) in Figure 6, plastic deformation in the as-casted and 1700 °C annealed Mo3Nb should be dominated by various slip systems because only one group of slip systems could not have α. In the as-casted Mo6Nb, as shown in Figure 6c, the fracture surface with β + γ occurs, which contributed to the slip in both the (121) <1$\bar{1}$1> and (110)<1$\bar{1}$1> systems. After annealing at 1700 °C, only the fracture surface with β was

observed, i.e., the slip in the (121) <1$\bar{1}$1> system was constricted. The addition of Nb changes the preference of the slip system. The (110)<1$\bar{1}$1> system is preferred in MoNb single crystal with low Nb content. In high Nb content MoNb single crystals, however, the (121) <1$\bar{1}$1> system is preferred at room temperature tensile tests with loading direction 111. In short, the critical resolved shear stress in the (110)<1$\bar{1}$1> system is enhanced by increasing Nb, which could be discussed further in future work.

As shown in Figure 4, deformation features are distinguishing among Mo, Mo3Nb, and Mo6Nb single crystals. The deformation features in Mo3Nb are nearly the same as in the Mo single crystals, as shown in Figure 4a,b, except for a stress drop after yield in Mo3Nb. Such a difference may be contributed to by the dislocation extending unstably after yield in Mo3Nb, i.e., the activation energy for dislocation extension is lower than for dislocation nucleation in Mo3Nb. What is more, the stress drop may be caused by the content fluctuation in as-casted Mo3Nb single crystals, as shown in Figure 8a. Dislocations are pinned by Nb atoms in the elastic deformation region. Then, dislocations de-pin and move when yield happens. A stress drop occurs when solute atoms distribute un-uniformly.

Work-hardening behaviors are nearly the same in Mo3Nb and Mo single crystals. Work-hardening in BCC metals at room temperature is mainly attributed to dislocation substructure [26], collective motion, and the interaction of dislocations [27]. As shown in the insert Figure 6(a-I), severe necking happens in Mo3Nb single crystals with a thin line in the fracture surface. As the Nb content rises, the work-hardening is much less (~0) in Mo6Nb than in Mo3Nb, as shown in Figure 4f. The yield stress is similar to the ultimate tensile strength of Mo6Nb, meaning a relatively stable dislocation extension at room temperature. Further research is necessary to reveal the effect of Nb on nucleation and the extension of dislocations in MoNb single crystals.

By adding Nb to Mo, the yield strength increases from ~250 MPa in Mo to ~450 MPa in Mo6Nb single crystals. Meanwhile, the ductility of as-casted single crystals does not change so much by adding Nb. For example, Mo single crystals have a ductility of ~10%, which is similar to Mo3Nb and Mo6Nb, which may be attributed to the same crystal growth methods and the distribution of residual stress and structural defects.

After annealing, the ductility in Mo3Nb and Mo6Nb are both effectively enhanced. For example, the ductility in the 1700 °C annealed Mo6Nb is enhanced to ~17%, which is much higher than ~10%. As shown in Figure 8, Nb distributes more uniformly after annealing at 1700 °C than the as-casted sample, meaning residual stress and structural defects are removed to a large extent. The unstable propagation of cracks may be delayed as growing stress relaxes after annealing.

One noted point is that strength in Mo3Nb single crystals drops from 420 MPa to 380 MPa, whereas the elongation visibly enhanced from 9% to 15.5% after annealing at 1300 °C, as shown in Figure 5c. Combining the stress drop behavior and content distribution of as-casted Mo3Nb single crystals, Nb atoms distribute less uniformly in as-casted Mo3Nb than in as-casted Mo6Nb. High growth stress concentration leads to relatively high strength and low elongation in as-casted Mo3Nb. It may be hard for growth stress to totally relax when annealing at 1100 °C. Growth stress may be totally relaxed due to enhanced atomic diffusion when annealing at a proper temperature (1300 °C). In this situation, elongation/strength effectively enhances/decreases. As the annealing temperature continually rises (1500 °C and 1700 °C), the low-angle grain boundary further eliminates due to fast atomic diffusion. As shown in Figure 7b, dislocation density decreases after annealing at 1700 °C, which causes the strength to further rise. Thus, choosing a proper annealing temperature is vital to determine the evolution of strength and ductility.

5. Conclusions

The mechanical properties of Mo and MoNb single crystals before and after thermal annealing were tested via tension at room temperature. With the addition of Nb, the strength of the Mo single crystal has been effectively enhanced and the fracture feature has been changed from severe necking to local shear. Furthermore, the work-hardening

ability notably drops to zero in Mo6Nb single crystals, suggesting stable flow under tension. After thermal annealing at 1100 °C, 1300 °C, 1500 °C, and 1700 °C, respectively, for 2 h, the ductility in MoNb single crystals is enhanced to a large extent. Based on the structural details by TEM and EDS, the distribution of Nb content is more uniform in the annealed sample than in the as-casted sample. In summary, the mechanical properties, especially the ductility of MoNb single crystals, are significantly improved via thermal annealing, which could be useful for increasing the reliability of MoNb single crystals at room temperature.

6. Patents

202211496675.0 (submitted).

Author Contributions: Conceptualization, L.H. and W.Z.; methodology, Z.H.; validation, T.Y., L.G. and H.Z.; writing—original draft preparation, L.H.; writing—review and editing, W.Z. All authors have read and agreed to the published version of the manuscript.

Funding: This research was funded by Northwest Institute for Nonferrous Metal Research, YK2102 and Major Special Science and Technology in Shaanxi Province, 2020zdzx04-02-02.

Data Availability Statement: The data that support the findings of this study are available from the corresponding author, upon reasonable request.

Acknowledgments: We acknowledge Northwest Institute for Nonferrous Metal Research and Major Special Science and Technology in Shaanxi Province.

Conflicts of Interest: The authors declare no conflict of interest.

References

1. El-Genk, M.S.; Tournier, J.M. A review of refractory metal alloys and mechanically alloyed-oxide dispersion strengthened steels for space nuclear power systems. *J. Nucl. Mater.* **2005**, *340*, 93–112. [CrossRef]
2. Majumdar, S.; Raveendra, S.; Samajdar, I.; Bhargava, P.; Sharma, I. Densification and grain growth during isothermal sintering of Mo and mechanically alloyed Mo–TZM. *Acta Mater.* **2009**, *57*, 4158–4168. [CrossRef]
3. Jiao, B.; Zhao, Q.; Zhao, Y.; Li, L.; Hu, Z.; Gao, X.; Zhang, W.; Li, J. The relationship between slip behavior and dislocation arrangement for large-size Mo-3Nb single crystal at room temperature. *J. Mater. Sci. Technol.* **2021**, *92*, 208–213. [CrossRef]
4. Majumdar, S.; Sharma, I.G.; Suri, A.K. Development of oxidation resistant coatings on Mo-30W alloy. *Int. J. Refract. Met. Hard Mater.* **2008**, *26*, 549–554. [CrossRef]
5. Sturm, D.; Heilmaier, M.; Schneibel, J.; Jéhanno, P.; Skrotzki, B.; Saage, H. The influence of silicon on the strength and fracture toughness of molybdenum. *Mater. Sci. Eng. A* **2007**, *463*, 107–114. [CrossRef]
6. Dimiduk, D.M.; Perepezko, J.H. Mo-Si-B alloys: Developing a revolutionary turbine-engine material. *Mater. Res. Soc. Bull.* **2003**, *9*, 639–645. [CrossRef]
7. Chen, X.; Li, R.; Li, B.; Wang, J.; Wang, T.; Yan, F.; Zhang, G. Achieving ultra-high ductility and fracture toughness in molybdenum via Mo2TiC2 MXene addition. *Mater. Sci. Eng. A* **2021**, *818*, 141422. [CrossRef]
8. Liu, G.; Zhang, G.J.; Jiang, F.; Ding, X.; Sun, Y.J.; Sun, J.; Ma, E. Nanostructured high-strength molybdenum alloys with unprecedented tensile ductility. *Nat. Mater.* **2013**, *12*, 344–350. [CrossRef]
9. Wang, L.; Sun, J.; Liu, G.; Sun, Y.; Zhang, G. Influences of annealing temperature on microstructure and mechanical properties of Mo–La_2O_3. *Int. J. Refract. Met. Hard Mater.* **2011**, *29*, 522–527. [CrossRef]
10. Wang, D.; He, D.; Li, K.; Wu, Z. Preparation and in-situ strengthening mechanisms of Mo composites with the addition of WC. *Mater. Sci. Eng. A* **2022**, *848*, 143478. [CrossRef]
11. Jing, K.; Liu, R.; Xie, Z.; Ke, J.; Wang, X.; Fang, Q.; Liu, C.; Wang, H.; Li, G.; Wu, X. Excellent high-temperature strength and ductility of the ZrC nanoparticles dispersed molybdenum. *Acta Mater.* **2022**, *227*, 117725. [CrossRef]
12. Lundgren, C.; Georgieva, A.K.; Gueorguiev, G.K. A perspective on thermal stability and mechanical properties of 2D Indium Bismide from ab initio molecular dynamics. *Nanotechnology* **2022**, *33*, 335706. [CrossRef]
13. Kakanakova-Georgieva, A.; Ivanov, I.G.; Suwannaharn, N.; Hsu, C.-W.; Cora, I.; Pécz, B.; Giannazzo, F.; Sangiovanni, D.G.; Gueorguiev, G.K. MOCVD of AlN on epitaxial graphene at extreme temperatures. *Crystengcomm* **2020**, *23*, 385–390. [CrossRef]
14. Yang, L.; Zhang, Q.; He, Z.; Li, X. Influences of HfC particles on microstructure, mechanical properties and ablation resistance at elevated temperature of Mo-15W-HfC alloys. *Int. J. Refract. Met. Hard Mater.* **2017**, *67*, 56–67. [CrossRef]
15. Zhang, H.; Zheng, J.; Yang, Q.; Zhang, Z.; Li, K.; Zhao, J.; Hu, Z.; Rao, L. Influence of Niobinum content on high temperature inner pressure creep resistance of Mo-Nb alloy aingle crystal. *Rare Metal Mater. Eng.* **2013**, *42*, 751–755.
16. Zhang, Q.; Li, Z.; Zheng, Y.; Zhang, J.; Hu, Z.; Zhang, T.; Yin, T.; Ding, X.; Ding, X. Develop of big of size Molybdenum-Niobium single crystal. *Rare Metal Mater. Eng.* **2005**, *34*, 1948–1951.

17. Jiao, B.; Zhao, Q.; Zhao, Y.; Zhang, W.; Li, Y.; Hu, Z.; Gao, X.; Cui, C.; Wu, M.; Xin, T. A new approach to understand the deformation behavior and strengthening mechanism of molybdenum alloy: From single crystal to polycrystal. *Int. J. Refract. Met. Hard Mater.* **2021**, *102*, 105715. [CrossRef]
18. Jiao, B.; Zhao, Q.; Zhao, Y.; Zhang, W.; Zhang, W.; Li, Y.; Hu, Z.; Gao, X.; Cui, C. Improving mechanical properties and achieving structural stability of large-size molybdenum single crystal during hot deformation by adding Nb element. *J. Alloy. Compd.* **2023**, *945*, 169369. [CrossRef]
19. Oehlerking, F.; Stawovy, M.T.; Ohm, S.; Imandoust, A. Microstructural characterization and mechanical properties of additively manufactured molybdenum and molybdenum alloys. *Int. J. Refract. Met. Hard Mater.* **2022**, *109*, 105971. [CrossRef]
20. Lowry, M.; Kiener, D.; LeBlanc, M.; Chisholm, C.; Florando, J.; Morris, J.; Minor, A. Achieving the ideal strength in annealed molybdenum nanopillars. *Acta Mater.* **2010**, *58*, 5160–5167. [CrossRef]
21. Yang, S.; Kou, H.; Zhang, G.; Liu, G.; Jiang, F.; Sun, J. Microstructural characterization of Mo–12Si–8.5B alloy subjected to diffusion annealing treatment. *Int. J. Refract. Met. Hard Mater.* **2010**, *28*, 377–382. [CrossRef]
22. Hiraoka, Y. High-temperature annealing embrittlement of single-crystalline molybdenum joined by using Mo-40% Ru alloy. *Int. J. Refract. Met. Hard Mater.* **2011**, *2*, 89–95. [CrossRef]
23. Grőger, R.; Racherla, V.; Bassani, J.L.; Vitek, V. Multiscale modeling of plastic deformation of molybdenum and tungsten: II. Yield criterion for single crystals based on atomistic studies of glide of 1/2111 screw dislocations. *Acta Mater.* **2008**, *56*, 5412–5425. [CrossRef]
24. Xu, S.; Xie, D.; Liu, G.; Ming, K.; Wang, J. Quantifying the resistance to dislocation glide in single phase FeCrAl alloy. *Int. J. Plast.* **2020**, *132*, 102770. [CrossRef]
25. Weinberger, C.R.; Boyce, B.L.; Battaile, C.C. Slip planes in bcc transition metals. *Int. Mater. Rev.* **2013**, *58*, 296–314. [CrossRef]
26. Irwin, G.J.; Guiu, F.; Part, P.L. Slip and Strain Hardening of Mo Single Crystals. *Phys. Stat. Sol.* **1974**, *685*, 22.
27. Lawley, A.; Gaigher, H.L. Deformation structures in zone-melted molybdenum. *Philos. Mag.* **1964**, *10*, 15–33. [CrossRef]

Disclaimer/Publisher's Note: The statements, opinions and data contained in all publications are solely those of the individual author(s) and contributor(s) and not of MDPI and/or the editor(s). MDPI and/or the editor(s) disclaim responsibility for any injury to people or property resulting from any ideas, methods, instructions or products referred to in the content.